# Magnetite nanoparticles enable a rapid conversion of volatile fatty acids to methane

Zhiman Yang, Rongbo Guo* Xiaoshuang Shi, Chuanshui Wang, Lin Wang, Meng Dai,

Shandong Industrial Engineering Laboratory of Biogas Production & Utilization, Key Laboratory of Biofuels, Qingdao Institute of Bioenergy and Bioprocess Technology, Chinese Academy of Sciences, Qingdao, Shandong Province 266101, P.R. China

*Corresponding author: E-mail: guorb@qibebt.ac.cn

## Supplementary Figures

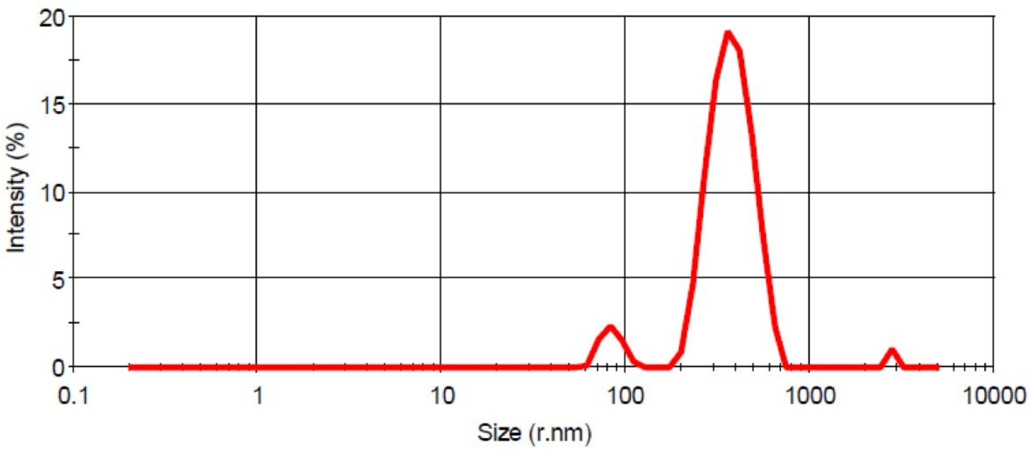


Figure S1. The distribution of particle size for synthesized magnetite. The particle size was analyzed with Zetasizer Nano S90.

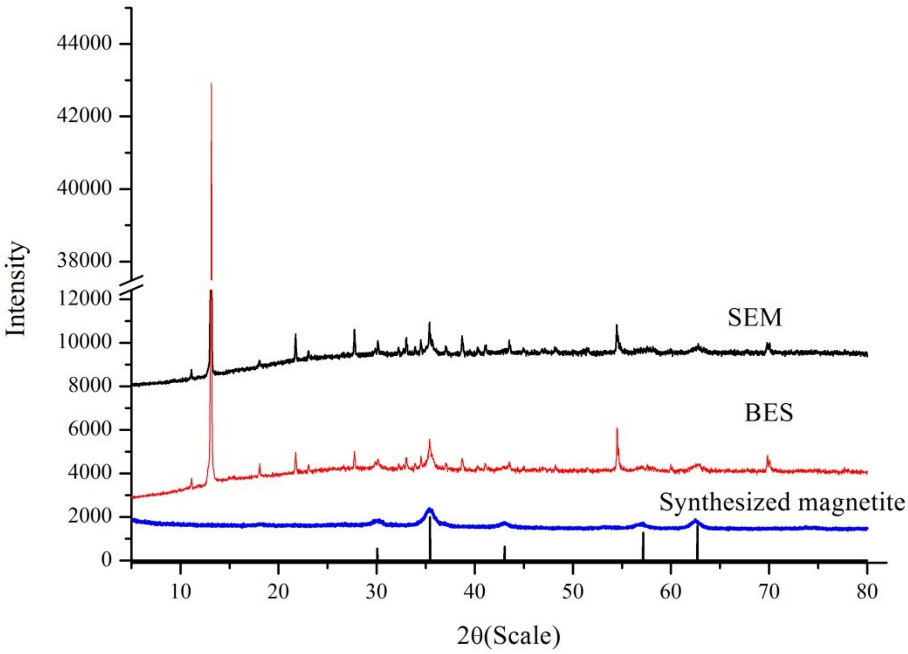


Figure S2. The X ray diffraction spectra of synthesized magnetite and its transformation product at the end of incubation. The pattern of products were similar with the standard value of Fe $(II)_3(PO_4)_2 \cdot 8H_2O$ (00-030-0662). The pattern of synthesized magnetite was same to the standard value of $Fe_3O_4$ (00-001-1111).

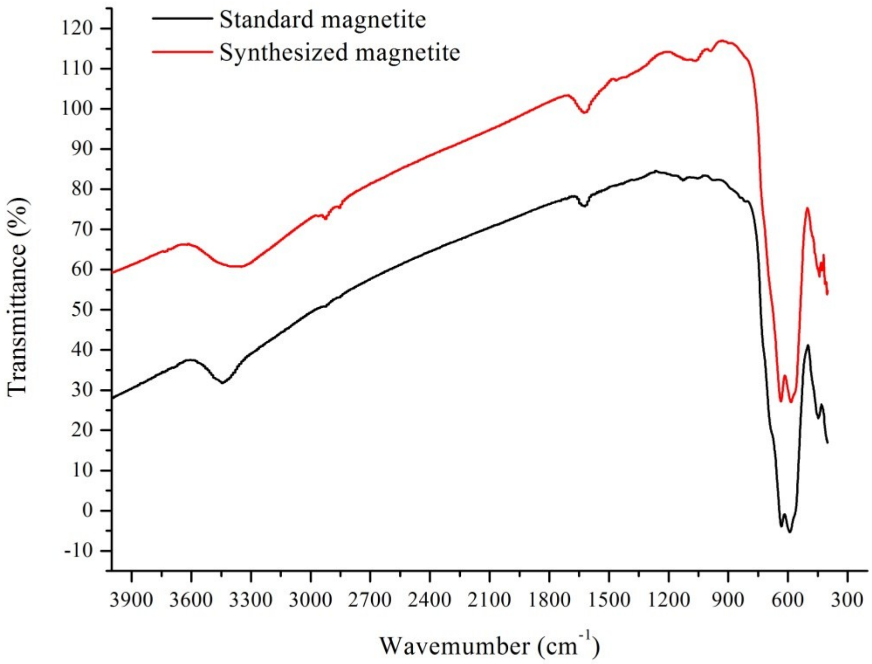


Figure S3. FTIR spectra of synthesized magnetite. The standard magnetite was purchased from Sigma-Aldrich Co. LLC. FTIR spectra of magnetite were analyzed using Fourier transform infrared spectroscopy (Nicolet 6700).

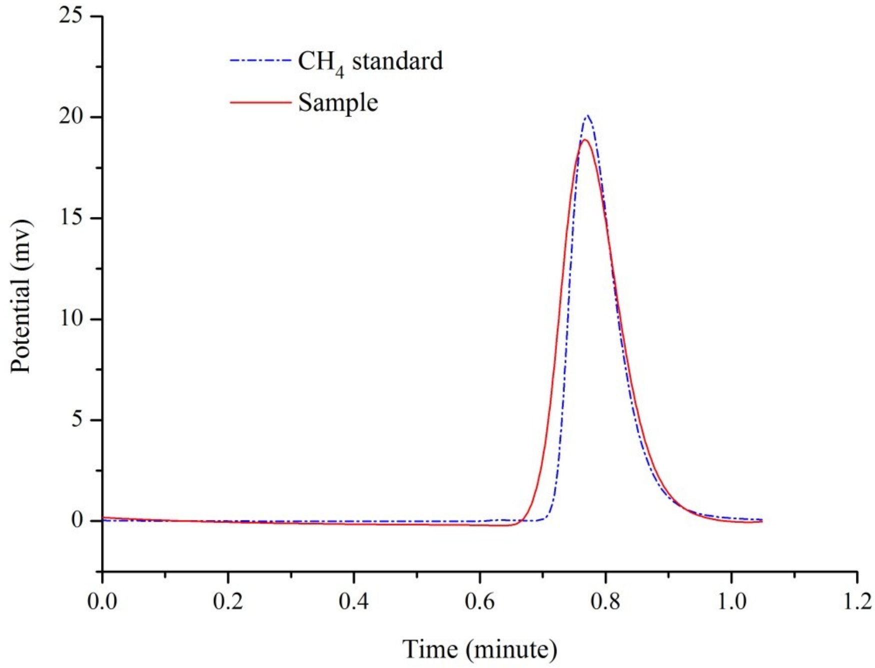


Figure S4. Representative gas chromatograms of methane standard and experimental sample.

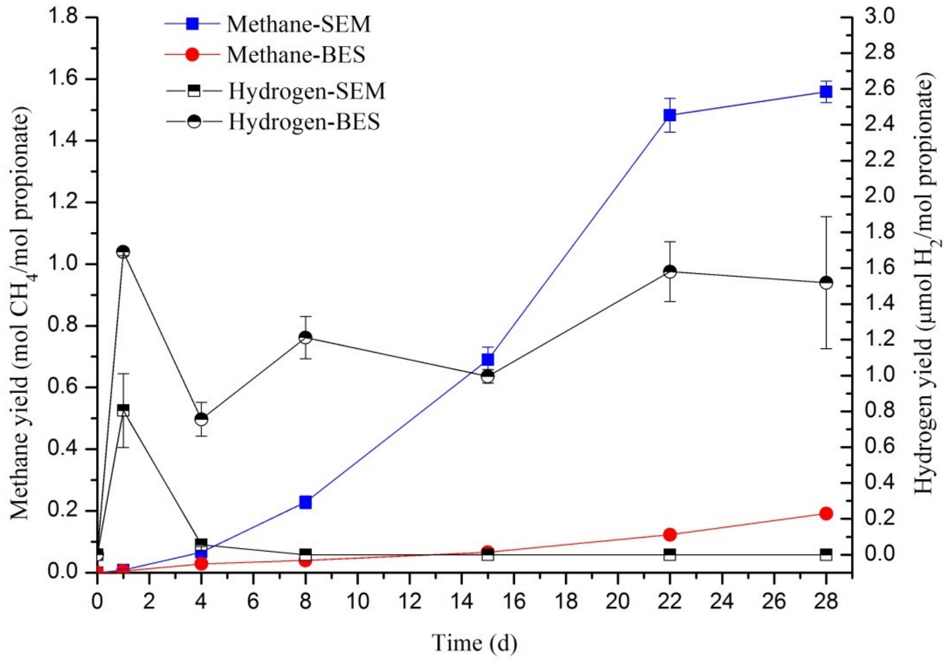


Figure S5. Changes of hydrogen and methane production in the presence of BES.

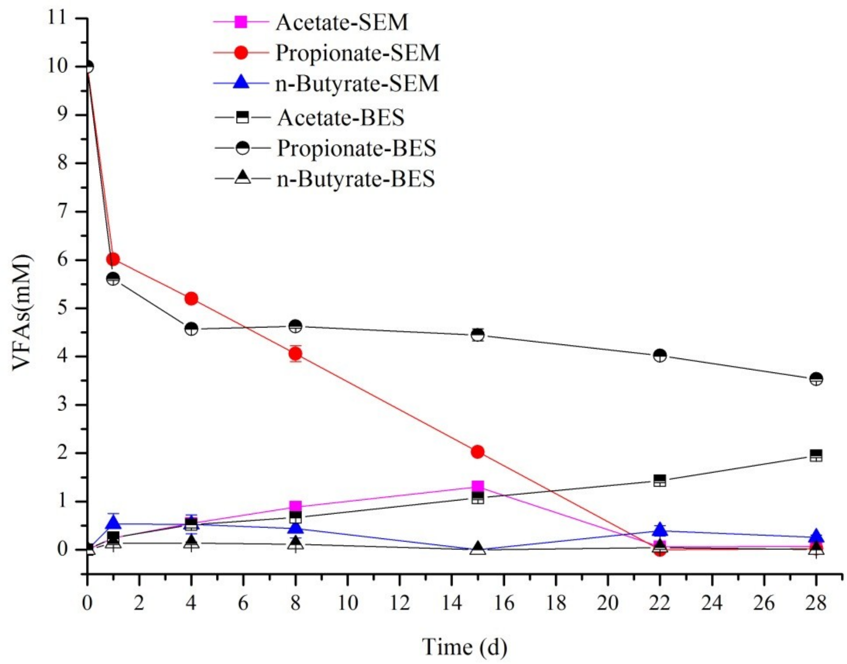


Figure S6. Changes of metabolites in the presence of BES.

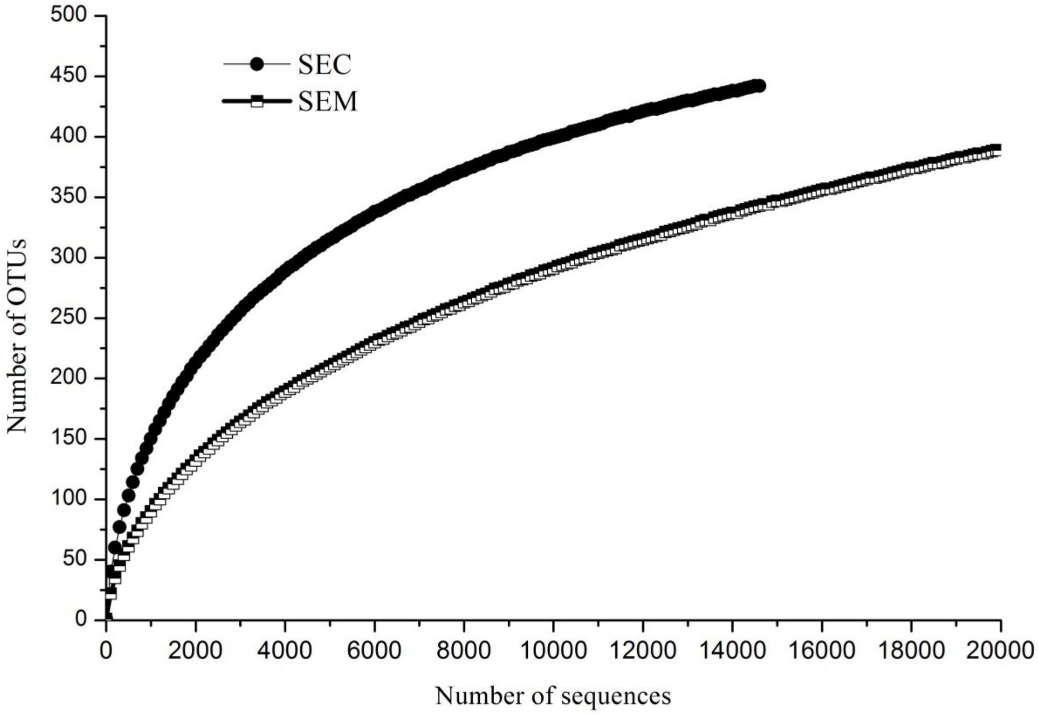


Figure S7. Rarefaction curves for bacterial community.

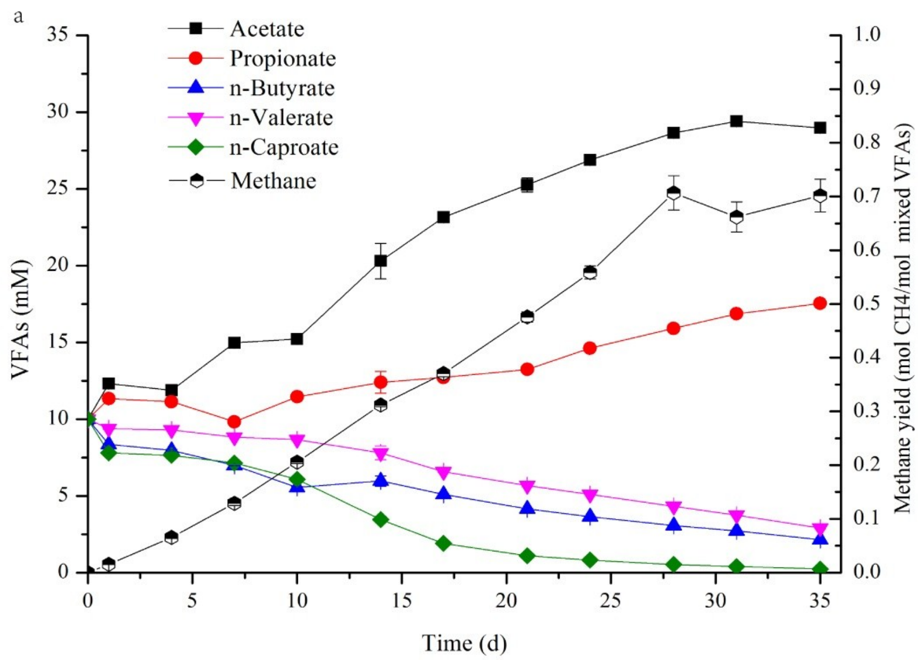


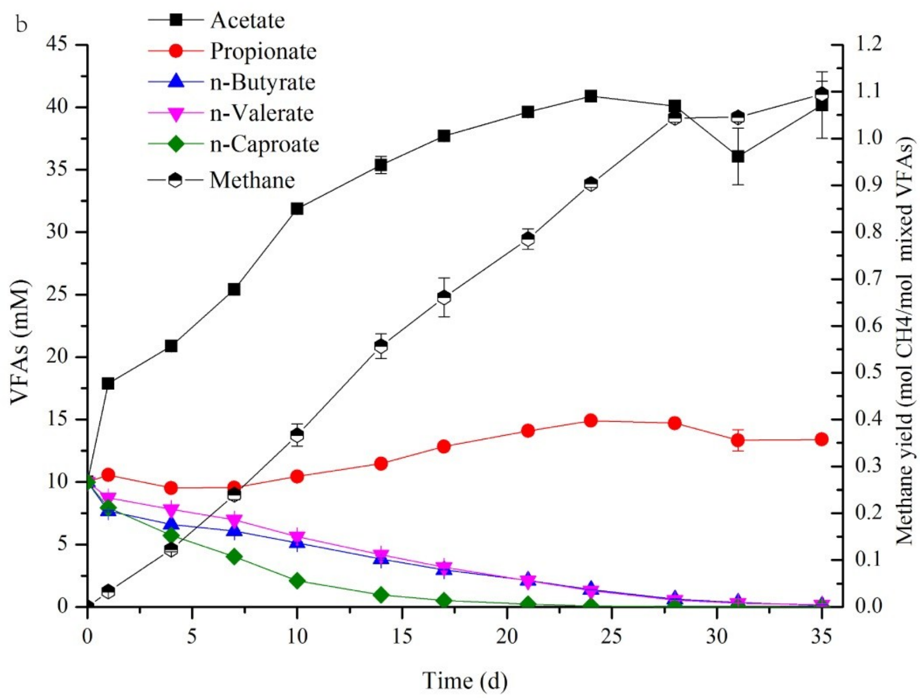


Figure S8. The time course of the production for both methane and metabolic intermediates during the cycle 1. a: SEC; b: SEM.

**Supplementary Tables**

Table S1. Kinetic parameters for methane production at different initial magnetite concentrations.

| Magnetite(mM) | Rm(mmol/d) | λ(d) | Ps(mol $CH_4$/mol-propionae) | $R^2$ |
|---|---|---|---|---|
| 20 | 0.066 | 1.91 | 1.66 | 0.99 |
| 80 | 0.067 | 1.88 | 1.70 | 0.99 |
| 160 | 0.064 | 2.41 | 1.66 | 0.99 |
| 320 | 0.063 | 3.15 | 1.68 | 0.99 |

Table S2. Concentration of initial undissociated propionic acid and kinetic parameters for methane production at different initial propionate concentrations.

| Propionate (mM) | Undissociated propionic acid (mM)[a] | Rm (mmol/d) | λ (d) | Ps (mol $CH_4$/mol-propionae) | $R^2$ |
|---|---|---|---|---|---|
| 10 | 0.074 | 0.078 | 1.99 | 1.58 | 0.99 |
| 20 | 0.147 | 0.097 | 3.18 | 1.30 | 0.99 |
| 50 | 0.368 | 0.096 | 6.40 | 1.20 | 0.99 |
| 100 | 0.736 | 0.111 | 13.12 | 1.42 | 0.99 |

[a] Calculated by using a $pK_a$ of 4.87 at 30°C and pH 7.

Table S3. Reactions involved in syntrophic degradation processes.

| | Reaction | $\Delta G^{0\prime}$(KJ per reaction)* |
|---|---|---|
| (1) | $CH_3CH_2COO^- + 3H_2O \rightarrow CH_3COO^- + HCO_3^- + H^+ + 3H_2$ | +76.1 |
| (2) | $CH_3(CH_2)_2COO^- + 2H_2O \rightarrow 2CH_3COO^- + H^+ + 2H_2$ | +48.1 |
| (3) | $CH_3(CH_2)_3COO^- + 2H_2O \rightarrow CH_3COO^- + CH_3CH_2COO^- + H^+ + 2H_2$ | +25.1 |
| (4) | $CH_3(CH_2)_4COO^- + 3H_2O \rightarrow 3CH_3COO^- + 2H^+ + 4H_2$ | +96.2 |
| (5) | $4H_2 + HCO_3^- + H^+ \rightarrow CH_4 + 3H_2O$ | -135.6 |

* $\Delta G^{0\prime}$ is calculated for standard conditions

Table S4. The richness and diversity of the bacterial community irrespective of the non-specific amplification sequences.

| | OTUs | Coverage (%) | CHAO1 richness estimation | Shannon diversity |
|---|---|---|---|---|
| SEC | 442 | 97 | 577 | 3.81 |
| SEM | 389 | 98.1 | 555 | 2.18 |